Chinese Chemical Letters 31 (2020) 2835–2838

Contents lists available at ScienceDirect

Chinese Chemical Letters

journal homepage: www.elsevier.com/locate/cclet

Communication

Adsorption of cesium using mesoporous silica gel evenly doped by Prussian blue nanoparticles

Tianyu Yuan, Qingde Chen, Xinghai Shen*

Beijing National Laboratory for Molecular Sciences, Fundamental Science on Radiochemistry and Radiation Chemistry Laboratory, Center for Applied Physics and Technology, College of Chemistry and Molecular Engineering, Peking University, Beijing 100871, China

ARTICLE INFO

Article history:
Received 21 January 2020
Received in revised form 16 February 2020
Accepted 12 March 2020
Available online 28 May 2020

Keywords:
Prussian blue
Mesoporous silica gel
Cesium
Adsorption
Radioactive wastewater

ABSTRACT

In this paper, a novel mesoporous silica gel evenly doped by Prussian blue nanoparticles (PBMSG) was successfully synthesized by using *N*,*N*-dimethylamide as template with a large Barrett-Emmett-Teller (BET) surface area of 505 m^2/g and an average pore size of 2.9 nm. The static adsorption experiments showed that the equilibration time of PBMSG for Cs^+ was about 30 min. The adsorption isotherm of PBMSG for Cs^+ accorded with Langmuir model and the theoretical maximum adsorption capacity was 80.0 ± 2.9 mg/g. When the initial concentration of Cs^+ was 1.00 mg/L, the adsorption partition coefficient K_d could reach 3.5×10^4 mL/g After adsorption, Cs^+ could be eluted by dilute hydrochloric acid (pH 2) with an efficiency of 89.8%, while no K^+, Fe^{3+}, Fe^{2+} was eluted. PBMSG exhibited good selectivity toward Cs^+ and Rb^+. In the presence of high concentration of K^+, the selective adsorption of PBMSG could change the mass ratio of K^+, Rb^+ and Cs^+ from 96.63:0.83:1.00–1.12:0.73:1.00. The separation of Cs^+ and Rb^+ from K^+ with similar concentration (100 mg/g) was realized by column experiment. This indicated that PBMSG was suitable for rapid recovery of low concentration of rubidium and cesium from complex matrixes, such as wastewater and salt lake brine, *etc*.

The radioactive cesium (*e.g.*, ^{137}Cs) generated in human nuclear activities is usually treated as waste [1], which is of great concern in environment, public health, and safety aspects [2]. Indeed, radioactive cesium is a very useful radiation source in industry, agriculture, medical field, *etc*. Moreover, cesium has broad applications in the fields of solar cells, atomic clock, electronic devices, catalysis, bio-medicine and so on [3–7]. Besides ore minerals, a large amount of Cs exists in salt lakes and underground brines [8–10]. However, in the brines, Cs^+ is at trace concentration and always coexists with other alkali metal elements (*e.g.*, potassium and rubidium) with similar physicochemical properties, making the extraction much difficult. In the traditional exploitation of brine resources, almost all Cs were lost [10]. Recently, the utilization of the Cs resources attracted much attention. Zhang *et al.* [10] used partially saponified 4-*tert*-butyl-2-(α-methylbenzyl) phenol (*t*-BAMBP) dodecane solution to extract Cs^+ from a synthetic brine solution containing K^+. However, this process must be carried out at high alkalinity condition. Yang and co-workers [11] synthesized Cs^+ ion-imprinted polymer using carboxymethyl chitosan as functional monomer, which selectively extracted Cs^+ but with the adsorption equilibrium time of 6 h. Chen *et al.* [8] successfully prepared Prussian blue functionalized graphene/carbon fibers composite to recover Cs^+ from aqueous solutions, whose maximum adsorption capacity reached 81.24 mg/g at 25 °C and pH 7. Nevertheless, in the electrochemical elution process, 0.1 mol/L KCl solution was applied, leading to the mixing of Cs^+ and K^+ again.

Because ^{137}Cs is one of the key radioactive nuclides in nuclear waste, much effort was paid to the extraction of Cs^+. By far, many methods have been applied to extract Cs^+, such as adsorption [8,11–15], solvent extraction [10,16,17], chemical precipitation [18] and so forth. Among these methods, adsorption has the advantage of easy operation and high efficiency. In this field, it is most important to synthesize an adsorbent with excellent performance towards Cs^+. Wang and co-workers [19] have reviewed that insoluble ferric ferrocyanide (*i.e.*, Prussian blue, PB) and its analogues are regarded as promising adsorbents, and there have been some applications in the treatment of wastewater. However, their performances (*i.e.*, adsorption rate, adsorption capacity and mechanical property) are not good enough. With the exploration on the nano-sized PB and its analogues, the adsorption rate and capacity were improved obviously [20]. Nevertheless, the nanoparticles were easy to be lost owing to their intrinsic property, *i.e.*, easy colloidization in water. Thus, much effort was paid to load the

* Corresponding author.
E-mail address: xshen@pku.edu.cn (X. Shen).

https://doi.org/10.1016/j.cclet.2020.03.035
1001-8417/

nanoparticles on different materials such as carbon materials [8], polymer [9,13,21], and inorganic materials [22,23]. Although the loading technique could well solve the loss problem of the nanoparticles, the adsorption capacity and/or adsorption rate of the hybrid materials were always restrained [9,19,23]. Furthermore, in order to recover the adsorbed Cs^+, high concentrations of KCl [8] or NH_4Cl-acid solution [24] were necessary, making the subsequent extraction of Cs^+ difficult. Therefore, there is still a great challenge.

Mesoporous silica gel (MSG, average pore diameter in the range of 2−50 nm) with high specific surface area and large mass transfer channels is an excellent substrate, which can be used in various environments. Some researchers used MSG as substrate to load PB for the recovering of Cs^+ [23,25]. However, the distribution of PB was not uniform, which made the low adsorption capacity. In order to evenly load materials and make full use of channels in MSG, the best choice is one-pot method. Nevertheless, the preparation of MSG was often confined in acidic or alkaline condition [26]. Wei and coworkers [27] used D-glucose as template to prepare MSG under near-neutral conditions, which made the loading of the acid and/or alkali sensitive materials possible.

At present, the research on the adsorption of Cs^+ in salt lake system is mainly with the following challenge: (1) Uniform loading of Prussian blue nanoparticles; (2) recovery of Cs^+ after adsorption; (3) separation of Cs^+ in the solution of high concentration K^+. Herein, we report the uniform immobilization of PB nanoparticles inside MSG, which can solve these problems.

Aqueous solutions of $Fe(NO_3)_3$ and $K_4Fe(CN)_6$ at 50 mmol/L were prepared, respectively. After mixing and stirring the two solutions with equal volume, a blue sol was obtained. Then, 7.2 mL blue sol, 16.6 mL tetraethyl orthosilicate (TEOS), 13.6 mL ethanol, 0.08 g concentrated HCl solution were added into a three-necked flask in turn. The homogeneous solution was obtained by stirring under N_2 atmosphere. Next, the solution was heated at 333 K for 2 h, into which 5 mL *N*,*N*-dimethylformamide (DMF) was added. After adjusting the pH value to 7 by 0.2 mol/L NaOH, the solution turned to a blue gel for a while. After lyophilization in vacuum, the silica was washed with deionized water. Finally, a dry Prussian blue nanoparticles (PBMSG) was obtained by lyophilization. The similar procedure only in the absence of blue sol was used to prepare MSG. At last, the dried adsorbent was sieved to get the particles between 80 and 200 mesh. The morphology of the nanoparticles and the element mapping images of hybrid silica were observed by transmission electron microscope (TEM, Tecnai-G2-F30, FEI, U. S. A.) and scanning electron microscope (SEM, JSM-IT300, JEOL, Japan). X-ray diffraction (XRD) pattern was recorded on Rigaku Dmax-2000 diffractometer (Japan) with Cu Kα radiation. X-ray photoelectron spectroscopy (XPS) of PBMSG before and after adsorption were collected on an ESCALAB 250Xi spectrometer (Thermo, U. S. A.), with monochromatized Al *K*α radiation, and the N_2 adorption-desorption isotherms were determined on a Micromeritics ASAP-2010 apparatus (U. S. A.).

The product *via* mixing $K_4Fe(CN)_6$ and $Fe(NO_3)_3$ solutions is composed of quasi-spherical nanoparticles with a diameter of about 10 nm (Fig. S1 in Supporting information), which is further determined to be cubic phase PB by the related XRD analysis (Fig. S2 in Supporting information). After co-gelation with silica, the SEM imaging of the PBMSG showed that the surface of PBMSG is significantly rougher than MSG (Fig. S3 in Supporting information), which indicate the loading of PB nanoparticles on the MSG. Furthermore, it can be found that the Fe element is uniformly distributed in the irregular silica gel particles from the typical element mapping images by TEM (Fig. S4 in Supporting information), indicating the successful even loading of PB nanoparticles.

In the N_2 adsorption-desorption isotherm of PBMSG and MSG, there appears an obvious hysteresis loop (curve a, Fig. S5 in Supporting information) associated with the filling of the mesoporous. The calculated Barrett-Emmett-Teller (BET) surface area, pore volume and pore size of PBMSG were 505 m^2/g, 0.37 cm^3/g and 2.4 nm, respectively. With respect to the MSG, it has a similar isotherm (curve b, Fig. S5 in Supporting information), and the corresponding parameters were determined to be 758 m^2/g, 0.45 cm^3/g and 2.9 nm, respectively. Obviously, both of them have mesoporous structure, whose pore volumes, pore sizes as well as pore size distributions (inset, Fig. S5 in Supporting information) are close to each other. The N_2 sorption isotherms of the materials belong to type IV isotherm adsorption curve according to IUPAC classification. This is due to the capillary phenomenon caused by the presence of mesoporous structure, which makes the constant adsorption capacity phenomenon appear in high partial pressure range. Moreover, the BET surface area of PBMSG became smaller than that of the blank MSG, suggesting the successful immobilization of PB nanoparticles in the MSG.

The corresponding XPS analysis (Fig. S6 in Supporting information) shows that the binding energies of C 1s and N 1s are 284.8 eV and 400.2 eV, respectively, which are close to the values of C≡N reported in the literature [28,29]. Fig. S6 (Supporting information) illustrates the spectrum in Fe 2p region, which consists of three peaks. The lower binding energy components at 708.9 eV and 712.3 eV comprise the Fe $2p_{3/2}$ signals and the other at 724.1 eV corresponds to Fe $2p_{1/2}$ [30–32]. Meanwhile, the peaks at 708.9 eV and 712.3 eV can be assigned to Fe(III) and the 724.1 eV to Fe(II) [30,31]. Thus, the generation of PB can be further demonstrated. There exist O 1s and Si 2p signals at the binding energy of 532.8 eV and 103.7 eV, similar to the literature value of silicon dioxide [33]. Moreover, the peak at 286.2 eV of C 1s and the peak at 531.2 eV of O 1s approach to the literature values of C-O [34] and Fe-O [35], respectively, which can explain the mechanism of MSG doped by PB. Furthermore, Argon ion was used to etch the surface of PBMSG (3000 eV, t = 10 s). The atom contents of Fe element on the surface and inside (after argon ion was used to etch the surface of PBMSG) of PBMSG were close (surface: 0.40%, inside: 0.33%). This indicated that MSG was evenly doped by PB nanoparticles. According to the above results, it can be concluded that the obtained hybrid material is mesoporous silica gel evenly doped by PB nanoparticles.

As shown in Fig. S7 (in Supporting information), when the initial concentration of Cs^+ is 100 mg/L, the adsorption rate of PBMSG is so fast that a relatively high capacity (90% of the equilibrium capacity) is obtained within 10 min. The adsorption equilibrium is realized at 30 min, due to the quick adsorption performance of nano-sized PB particles and the quick mass transfer of mesoporous structure. In order to ensure the adsorption equilibrium at other initial concentrations of Cs^+, the adsorption time was chosen to be 2 h in the following studies.

The adsorption capacity of MSG and PBMSG increases with an increase in the equilibrium concentration of Cs^+ (Fig. S8 in

Table 1
Fitting results of the Langmuir and Freundlich models.

	Langmuir		
	q_m (mg/g)	B (L/mg)	R^2
MSG	36.3 ± 3.6	$(7 \pm 2)\times10^{-3}$	0.92
PBMSG	80.0 ± 2.9	$(4 \pm 0.4)\times10^{-3}$	0.99
	Freundlich		
	$1/n$	K [(mg/g)·(L/mg)$^{1/n}$]	R^2
MSG	3.1 ± 0.9	3.5 ± 2.1	0.72
PBMSG	2.1 ± 0.2	2.4 ± 0.7	0.95

Supporting information). The isothermal adsorption data were analyzed with the Langmuir and Freundlich models. The corresponding fitting results were presented in Fig. S8 (in Supporting information) and Table 1, which indicated that the Langmuir model is more suitable than Freundlich model. The q_m value of PBMSG calculated by Langmuir model was 80.0 ± 2.9 mg/g, which was larger than other traditional materials doped with PB [9,19,36]. Compared with MSG, the adsorption capacity of PBMSG was significantly lager. This was an indication that the PB nanoparticles played an important role in the adsorption process. Although the PB nanoparticles were immobilized in different depth and the maximum loading of PB was only about 10 mg/g, the adsorption capacity of PBMSG was still large enough. Moreover, the distribution coefficient K_d increases gradually with the decrease of initial concentration of Cs^+ (Fig. S9 in Supporting information). The K_d could reach 3.5×10^4 mL/g at an initial Cs^+ concentration of 1.00 mg/L. Furthermore, comparing the atom contents of Cs element on the surface and inside (after argon ion was used to etch the surface of PBMSG) of the PBMSG after adsorption *via* XPS analysis (Fig. 1), the values (surface: 0.33%, inside: 0.17%) indicated that the PB nanoparticles immobilized in MSG were effective during adsorption process.

The effect of acidity on the adsorption was investigated by altering the pH value from 5.8 to 2.2 by HCl solution (Fig. S10 in Supporting information). After the pH value decreases to 3.5, the adsorption capacity of PBMSG decreases obviously. When the pH value reaches 2.2, PBMSG cannot adsorb any Cs^+. This phenomenon suggested that the adsorbed Cs^+ may be desorbed by adjusting acidity.

After adsorption, 20 mg PBMSG (*Q*: 25.50 mg/g) was added into 20 mL HCl solution (pH 2). Then, the mixture was shaken for 2 h at 298 K. In the eluate, the Cs^+ concentration was measured to be 22.90 mg/L (*i.e.*, the elution ratio of Cs^+ was 89.8%), while K, Fe and other elements were not found within the error of ICP-AES measurement. Considering the stability of PB [37], it can be guaranteed that the PBMSG does not release CN^- to the environment during usage. Although PB could be destroyed and gathered in the acid solution [38], comparing the XPS spectra of PBMSG before and after acid treatment (Fig. S11 in Supporting information), it is found that there are no significant changes in the structure of PB. It indicated that the structure of mesoporous could effectively prevent the outflow of interfering ions. In other words, the elution of Cs^+ adsorbed by PBMSG was easy and did not introduce other cation impurities, making the recovery of Cs^+ much simple. Compared with the materials using PB as adsorbents in recent years (Table S1 in Supporting information), PBMSG has the advantages of large adsorption amount, short adsorption time, and no introduction of other interfering ions during elution.

The adsorption selectivity of PBMSG and MSG has shown in Fig. S12 (in Supporting information). MSG has adsorption capacity of Cs^+, Rb^+ and K^+, but PBMSG only have the adsorption capacity of Cs^+ and Rb^+, which indicted the adsorption selectivity of PB nanoparticles. Moreover, 10.0 mg PBMSG was used to extract Cs^+ and/or Rb^+ from 5 mL mixed solution of Cs^+ and/or Rb^+ with K^+, where the concentrations of each ions were 100 mg/L. In all cases, K^+ is hardly adsorbed, while the adsorption of Cs^+ and/or Rb^+ is remarkable (Fig. S13 in Supporting information). In other words, Cs^+ and/or Rb^+ could be selectively adsorbed in the presence of K^+. Because the selectivity of PB was achieved by lattice defects [39], the similar adsorption properties of Cs^+ and Rb^+ could be attributed to their similar hydration radius.

In a static adsorption experiment, 20 mg PBMSG was applied to deal with 20 mL mixed solution of K^+, Rb^+ and Cs^+, whose concentrations were 1120, 9.58 and 11.59 mg/L, respectively. After being washed by HCl solution (pH 2), 20 mL desorption solution containing 11.00 mg/L K^+, 7.16 mg/L Rb^+ and 9.80 mg/L Cs^+ was obtained. Thus, after an adsorption-desorption process, most of K^+ was removed and the concentration of residual K^+ was similar to those of Rb^+ and Cs^+ Moreover, the adsorption kinetics of Cs^+ and Rb^+ in high concentration of K^+ were studied (Fig. 2). It can be seen from the figure that the adsorption rate of Cs^+ or Rb^+ is still very fast even in the presence of high concentration of K^+ (K^+ was not adsorbed). Therefore, the PBMSG was well suited for extracting small amounts of Cs^+ or Rb^+ from a solution with high concentrations of K^+.

Furthermore, in order to separate Cs^+ and Rb^+ from K^+ with close concentration, a column using PBMSG as adsorbent was packed, whose height and diameter were 3 cm and 1 cm, respectively. After adding a mixture solution of K^+, Rb^+ and Cs^+ (concentration of each ion was 25 mg/L), the column was eluted by deionized water and HCl solution (pH 3.5) with a rate of 2.5 mL/min in turn. The elution curve (Fig. 3) shows that most of K^+ was washed out after the mother solution was added, the residual K^+ was eluted by water. After HCl solution was applied, Rb^+ was firstly eluted, and then Cs^+ and Rb^+ appeared in the eluent simultaneously. In other words, a baseline separation of Cs^+ and Rb^+ from K^+ was realized by using the PBMSG column. As for the further separation of Cs^+ and Rb^+, we have obtained preliminary results through the modification of the materials and the optimization of the methods, which will be further reported in subsequent paper.

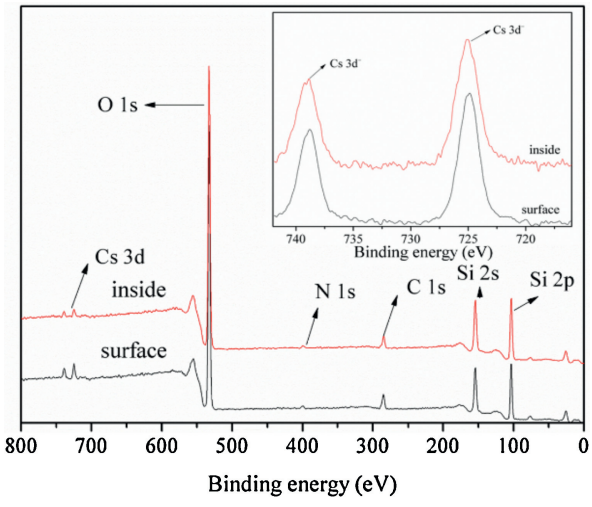

Fig. 1. The XPS spectrum of PBMSG after adsorbing Cs^+ (inset: the Cs 3d region).

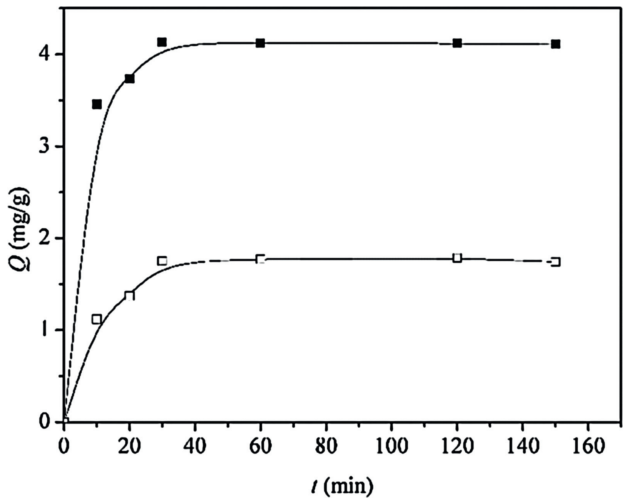

Fig. 2. The adsorption kinetics of Cs^+ and Rb^+ in the presence of high concentration of K^+ (Cs^+ (■), Rb^+ (□), C_0 (K^+) = 104 mg/L, C_0 (Cs^+) = 8.72 mg/L, C_0 (Rb^+) = 9.26 mg/L).

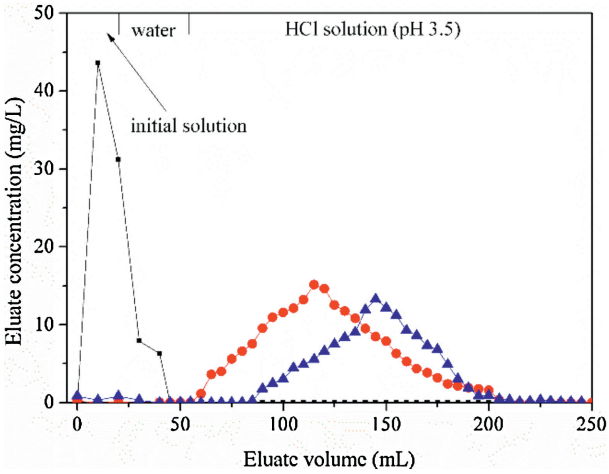

Fig. 3. Elution curve of PBMSG column in the separation of Rb^+/Cs^+ and K^+ (K^+ (■), Rb^+ (●) and Cs^+ (▲)).

In summary, by an improved sol-gel synthesis method and taking the advantage of the easy colloidization of PB nanoparticles, MSG evenly doped with PB nanoparticles was successfully synthesized, which has an excellent adsorption performance towards Cs^+. The adsorption rate of PBMSG towards Cs^+ was so fast that 90% of the equilibrium capacity was obtained within 10 min and adsorption equilibrium was realized at 30 min. The adsorption isotherm was fitted well with Langmuir model, and the maximum adsorption capacity reached 80.0 ± 2.9 mg/g. The K_d value reached 3.5×10^4 mL/g at an initial concentration of 1.00 mg/L and the adsorbed Cs^+ could be easily eluted by HCl solution (pH 2). Especially, PBMSG could selectively extract Cs^+ and Rb^+ from the solution containing high concentration of K^+. Moreover, the column with PBMSG as adsorbent was used to realize the baseline separation of Cs^+ and Rb^+ from K^+ with close concentration. Compared with other PB-based materials, the PBMSG had good performance in all aspects. In this work, the problem of load uniform and introduction of interfering ions during the elution process was solved. Therefore, it is reasonable to believe that PBMSG prepared in this work is promising in the rapid recovery of trace Cs^+ and Rb^+ from complex matrixes, such as wastewater and salt lake brine, *etc.*

Declaration of competing interests

We declare that they have no known competing financial interests or personal relationships that could have appeared to influence the work reported in this paper.

Acknowledgments

The authors are grateful to Dr. Zejun Li for the help in the ICP-AES measurement. This work was supported by National Natural Science Foundation of China (No. U1507203) and Science Challenge Project (No. TZ2016004).

Appendix A. Supplementary data

Supplementary material related to this article can be found, in the online version, at doi:https://doi.org/10.1016/j.cclet.2020.03.035.

References

[1] H. Kim, M. Kim, W. Lee, S. Kim, J. Hazard. Mater. 347 (2018) 106–113.
[2] A. Takahashi, A. Kitajima, D. Parajuli, et al., Chem. Eng. Res. Des. 109 (2016) 513–518.
[3] G.E. Eperon, T. Leijtens, K.A. Bush, et al., Science 354 (2016) 861–865.
[4] L.F. Peng, R.Z. Li, Z.L. Tang, et al., Tetrahedron 73 (2017) 3099–3105.
[5] Y.Y. Yu, X.M. Chen, Y. Jin, et al., J. Phys. D-Appl. Phys. 50 (2017) 275104–275111.
[6] N. Huntemann, B. Lipphardt, C. Tamm, et al., Phys. Rev. Lett. 113 (2014) 210802–210807.
[7] J. Zhong, W. Yao, W. Lee, Int. J. Dev. Neurosci. 25 (2007) 359–365.
[8] F.P. Chen, G.P. Jin, S.Y. Peng, X.D. Liu, J.J. Tian, Colloid Surf. A-Physicochem. Eng. Asp. 509 (2016) 359–366.
[9] Z. Jia, X. Cheng, Y. Guo, L. Tu, Chem. Eng. J. 325 (2017) 513–520.
[10] J. Zhang, L. Yang, T. Dong, et al., Ind. Eng. Chem. Res. 57 (2018) 4399–4406.
[11] L. Yang, S. Li, C.J. Sun, Dispersion Sci. Technol. 38 (2016) 1547–1555.
[12] C.Y. Chang, L.K. Chau, W.P. Hu, C.Y. Wang, J.H. Liao, Microporous Mesoporous Mater. 109 (2008) 505–512.
[13] G.R. Chen, Y.R. Chang, X. Liu, et al., Sep. Purif. Technol. 153 (2015) 37–42.
[14] S. Feng, X. Li, F. Ma, et al., RSC Adv. 6 (2016) 34399–34410.
[15] I.E. Burgeson, J.R. Deschane, B.J. Cook, D.L. Blanchard, D.L. Weier, Sep. Sci. Technol. 41 (2006) 2373–2390.
[16] S.M. Liu, H.H. Liu, Y.J. Huang, W.J. Yang, Trans. Nonferrous Met. Soc. China 25 (2015) 329–334.
[17] S. Nisan, F. Laffore, C. Poletiko, N. Simon, Desalin. Water Treat. 8 (2012) 236–245.
[18] S.G. Beheir, K. Benyamin, F.M. Mekhail, J. Radioanal. Nucl. Chem. 232 (1998) 147–150.
[19] J. Wang, S. Zhuang, Y. Liu, Coord. Chem. Rev. 374 (2018) 430–438.
[20] H. Sadegh, G.A.M. Ali, V.K. Gupta, et al., J. Nanostruct. Chem. 7 (2017) 1–14.
[21] Y.C. Lai, Y.R. Chang, M.L. Chen, Bioresour. Technol. Rep. 214 (2016) 192–198.
[22] M. Darder, Y. González-Alfaro, P. Aranda, E. Ruiz-Hitzky, RSC Adv. 4 (2014) 35415–35421.
[23] Y. Inaba, Y. Sakai, K. Kanazawa, et al., Chem. Lett. 45 (2016) 776–778.
[24] J.Y. Su, G.P. Jin, T. Chen, et al., Electrochim. Acta 230 (2017) 399–406.
[25] T. Sangvanich, V. Sukwarotwat, R.J. Wiacek, et al., J. Hazard. Mater. 182 (2010) 225–231.
[26] J.H. Clark, D.J. Macquarrie, S.J. Tavener, Dalton Trans. 36 (2006) 4297–4309.
[27] Y. Wei, J. Xu, H. Dong, S.A. Jansen-Varnum, Chem. Mat. 11 (1999) 2023–2029.
[28] A. Lisowska-Oleksiak, A.P. Nowak, M. Wilamowska, et al., Synth. Met. 160 (2010) 1234–1240.
[29] A.S. Kumar, P. Barathi, K.C.J. Pillai, Electroanal. Chem. 654 (2011) 85–95.
[30] M. Datta, A. Datta, J. Phys. Chem. 94 (1990) 8203–8207.
[31] J. Zhang, W. Yang, H. Zhu, et al., J. Colloid Interf. Sci. 338 (2009) 319–324.
[32] Q.T. Pan, K. Huang, S.B. Ni, F. Yang, D.Y. He, Mater. Res. Bull. 44 (2009) 388–392.
[33] A. Cros, R. Saoudi, G. Hollinger, C.A. Hewett, S.S. Lau, J. Appl. Phys. 67 (1990) 1826–1830.
[34] H. Willemen, L.F. Wuyts, D.F. Vandevondel, G.P. Vanderkelen, J. Electron Spectrosc. Relat. Phenom. 11 (1977) 245–250.
[35] H. Seyama, M.J. Soma, Chem. Soc.-Faraday Trans. 81 (1985) 485–495.
[36] H. Yang, H. Li, J. Zhai, H. Yu, Chem. Eng. J. 277 (2015) 40–47.
[37] P.A. Haas, Sep. Sci. Technol. 28 (1993) 2479–2506.
[38] T.R. Bolam, W. Taylor, Trans. the Faraday Soc. 35 (1939) 268–276.
[39] M. Ishizaki, S. Akiba, A. Ohtani, et al., Dalton Trans. 42 (2013) 16049–16055.